



Thermally Sprayed Coatings as Interlayers for DLC-Based Thin Films

G. Bolelli, E. Gualtieri, L. Lusvarghi, F. Pighetti Mantini, F. Pitacco, S. Valeri, and H. Volz

(Submitted September 5, 2008; in revised form October 27, 2008)

This article examines the usefulness of a thick thermally sprayed interlayer (plasma-sprayed Ni-50%Cr, plasma-sprayed Al_2O_3 -13% TiO_2 , or high-velocity oxygen-fuel-sprayed WC-17%Co) for enhancing the wear resistance and the corrosion protectiveness of a diamond-like carbon (DLC)-based thin film deposited onto a carbon steel substrate. Scratch tests indicate that the Al_2O_3 -13% TiO_2 and WC-17%Co interlayers definitely increase the critical spallation load of the thin film, but the Al_2O_3 -13% TiO_2 interlayer itself undergoes brittle fracture under high-contact loads. Accordingly, during ball-on-disk tests at room temperature, no cracking and spallation occur in the DLC-based film deposited onto the WC-17%Co interlayer, whereas the one onto the Al_2O_3 -13% TiO_2 interlayer is rapidly removed because the interlayer itself is fractured. At 300 °C, by contrast, the DLC-based film on the Al_2O_3 -13% TiO_2 interlayer offers the best tribological performance, possibly thanks to the increased toughness of the ceramic interlayer at this temperature. Electrochemical polarization tests indicate that the thin film/WC-Co systems possess the lowest corrosion current density.

Keywords coating-substrate interaction, corrosion and electrochemical behavior, friction and wear, scratch testing

1. Introduction

Diamond-like carbon (DLC) films generally combine high hardness and low-friction behavior. They are therefore extremely appealing for several industrial applications, e.g. protection of plastic injection moulds, coating of automobile parts, and of components for industrial plants, etc. (Ref 1-3). In those applications, DLC films deposited onto steel substrates can indeed reduce significantly the coated component's wear rate (up to 200 times lower than in uncoated conditions) and, most importantly, the friction coefficient (from 0.5 to 0.1, steel on steel, just one of the sliding bodies coated) (Ref 1, 2).

However, DLC films are intrinsically brittle and their thickness is limited to $<5 \mu\text{m}$ by various factors, including the generally low deposition rates of PVD and CVD techniques and the high levels of residual stresses in the deposited film (Ref 1). Due to their low thickness, DLC films cannot entirely carry the stress distribution generated by the contact between the coated component and its

counterpart. Consequently, the mechanical properties of the substrate also play an important role in determining the overall behavior of a DLC-coated component subjected to contact conditions. Specifically, as long as the substrate behaves elastically, the most influential factor is the ratio between the elastic moduli of the coating and of the substrate (Ref 4-6); however, when the stress in the substrate exceeds its yield strength, the coating is dramatically overloaded (Ref 4) and it can crack and/or delaminate (Ref 7-9). This problem may affect, for instance, carbon steel substrates, having suitably high modulus ($\approx 210 \text{ GPa}$) but limited hardness. Even larger troubles arise when using light alloys, with low hardness and low elastic modulus (Ref 7, 9).

In order to overcome these problems, a thick ($>100 \mu\text{m}$) interlayer having high hardness and modulus can be interposed between the DLC coating and a soft substrate. The contact stress distribution would indeed be borne by the hard interlayer, thus avoiding the troubles connected to the low yield strength of the substrate. "Duplex" systems, where DLC films or other hard thin-film coatings (like TiN) are deposited onto thick interlayers, have seldom been dealt with in the literature, although very promising results have been put forward (Ref 10-14).

In a previous article, the authors proposed thermal spraying as a viable technique for the production of such thick interlayers on a steel substrate, and suggested their usefulness for supporting DLC-based thin films deposited by electron cyclotron resonance-chemical vapor deposition (ECR-CVD) (Ref 15). Both ECR-CVD and thermal spraying, indeed, do not overheat the substrate (deposition temperatures can be kept to $<200 \text{ }^\circ\text{C}$); therefore, they can be applied to a wide range of substrate materials and geometries (Ref 16-18). Consequently, there are a large number of industrially relevant components to which

G. Bolelli, L. Lusvarghi, and F. Pighetti Mantini, Department of Materials and Environmental Engineering, Università degli Studi di Modena e Reggio Emilia, Via Vignolese 905, 41100 Modena, Italy; E. Gualtieri and S. Valeri, Department of Physics, Università degli Studi di Modena e Reggio Emilia, Via Campi 213/a, 41100 Modena, Italy; and F. Pitacco and H. Volz, Protec Surface Technologies S.r.l., Via Benaco, 88, 25081 Bedizzole, BS, Italy. Contact e-mails: giovanni.bolelli@unimore.it, bolelli.giovanni@unimore.it.

such “duplex” coating system can potentially be applied, because they can be treated both by ECR-CVD and by thermal spraying. Moreover, thermal spraying techniques offer an excellent flexibility in the selection of the interlayer material.

In order to provide a clear understanding of the actual benefits which the use of the thermally sprayed interlayers can produce in the adhesion and wear behavior of the DLC-based thin films, the present article deepens the preliminary microstructural and tribological characterization previously given in Ref 15. New tribological tests are performed, and the focused ion beam (FIB) technique is employed for characterizing both the as-deposited and the worn samples, in order to gain a deeper understanding of the behavior of these “duplex” systems. Moreover, the corrosion resistance of these systems is also investigated.

As reported in Ref 15, different kinds of thermally sprayed layers were tested: atmospheric plasma-sprayed (APS) Ni-50wt.%Cr, APS Al₂O₃-13wt.%TiO₂, and high-velocity oxygen-fuel (HVOF)-sprayed WC-17wt.%Co, which are representative of the three main categories of materials which are commonly employed in the thermal spray industry, namely metallic alloys, oxide ceramics, and cermets (Ref 16-18).

2. Experimental Procedure

2.1 Deposition of Thermal Spray Coatings

By using the APS process (Sulzer-Metco F4-MB plasma torch), a Ni-50%Cr (powder: Sulzer-Metco Amdry 350C, $-106+38\ \mu\text{m}$) coating and an Al₂O₃-13%TiO₂ (powder: Sulzer-Metco 130, $-53+15\ \mu\text{m}$) coating, the latter having a NiCoCrAlY bond coat (powder: Sulzer-Metco 461NS, $-150+22\ \mu\text{m}$) in order to improve its adhesion, were deposited onto grit-blasted C40 steel plates of $(100 \times 100 \times 5)\ \text{mm}^3$ size. A WC-17%Co (powder: Tafa 1343, $-45+15\ \mu\text{m}$) cermet coating was produced on the same substrate by the HVOF spraying process, using a Praxair-Tafa JP5000 torch. The deposition parameters are specified in Ref 15 (APS-NiCr), Ref 19 (APS-Al₂O₃-TiO₂), and Ref 20 (WC-Co). The thickness of all coatings is larger than 200 μm .

2.2 Deposition of DLC-Based Thin Films

A three-layer DLC-based thin film was deposited both on the bare C40 substrate and on the three thermally sprayed interlayers; the same deposition parameters were employed in all cases. The films consists of a thin (0.5 μm thick) Cr adhesive layer and a WC/C intermediate layer (1.5 μm thick), both produced by magnetron sputtering, and of a 2.5- μm -thick DLC top layer, produced by ECR-CVD (see layout in Fig. 1a). The deposition temperature was $<200\ ^\circ\text{C}$. More information on the film deposition is provided in [15], but details on the parameters are proprietary. It is important to remind that, prior to the deposition of the thin film, all surfaces were ground and then polished using 3- and 0.5- μm polycrystalline diamond

slurries. The average roughness R_a of the substrate should indeed be $\leq 0.2\ \mu\text{m}$ in order to avoid spallation of DLC-based films during sliding contacts (Ref 21). This polishing procedure was able to reduce the roughness of the C40 steel to $R_a \approx 0.02\ \mu\text{m}$ and that of HVOF-sprayed WC-Co to $R_a \approx 0.03\ \mu\text{m}$. The APS coatings, by contrast, contain a certain degree of porosity; consequently, their roughness after polishing is $R_a \approx 0.1\ \mu\text{m}$.

2.3 Characterization of the Coated Samples

The DLC-based thin films were sectioned and observed using a dual beam machine (StrataTMDB235, FEI, Eindhoven, The Netherlands) combining a high-resolution FIB column equipped with a Ga liquid metal ion source (LMIS) and a SEM column equipped with a Schottky field emission gun (SFEG) electron source. The section was produced by FIB using a 5 nA ion beam current and polished using a 300 pA ion beam current. A Pt layer was previously applied in order to protect the surface of the sample, assisting the local deposition by FIB (300 pA ion current). The sectioned surface was then observed using the SEM column (resolution up to 2 nm), under an angle of 52°.

The chemical composition of the DLC top layer was analyzed by X-ray photoelectron spectroscopy (XPS), as reported in Ref 22; in particular, the sp^3/sp^2 ratio was evaluated using the Auger structure in XPS spectra (XAES: X-ray excited Auger Electron Spectroscopy).

Depth-sensing Berkovich nanoindentation (Nano-Indentation Tester, CSM Instruments, Peseux, Switzerland), performed under a prescribed penetration depth of 200 nm, allowed the measurement of the nanohardness of the films, computed using the Oliver-Pharr procedure (Ref 23) (Poisson's ratio: 0.15). On each sample, 15 indentations were performed.

The scratch adhesion (Micro-Combi Tester, CSM Instruments) of the thin films was assessed according to ASTM C1624-05, performing scratch tests with a conical diamond indenter having a spherical tip (radius = 200 μm), operating with linearly increasing load in the 0.1-30 N range (15 N/min loading rate, 4 mm scratch length, two scratches for each sample). The critical loads L_{C1} (first crack in the scratch groove), L_{C2} (edge spallation), and L_{C3} (spallation inside the groove) were determined by optical microscopy inspection after scratching (Ref 24). The scratch grooves were also observed by SEM (XL30, FEI) equipped with energy dispersive X-ray spectrometry (EDX, INCA 350, Oxford Instruments, Abingdon, UK).

Using a pin-on-disk tribometer (High-Temperature Tribometer, CSM Instruments), unidirectional ball-on-disk tribological tests were performed in dry conditions on thin film-coated samples, according to ASTM G99-05. Sintered alumina balls (3 mm diameter, nominal hardness HV = 19 GPa) were employed as counterparts. Tests were performed at room conditions (temperature $(21 \pm 2)\ ^\circ\text{C}$, relative humidity $(55 \pm 2)\%$) and at 300 $^\circ\text{C}$, using a normal load of 10 N, a sliding speed of 30 cm/s and a total sliding distance of 5000 m. The wear rates of the samples were determined by optical confocal profilometry

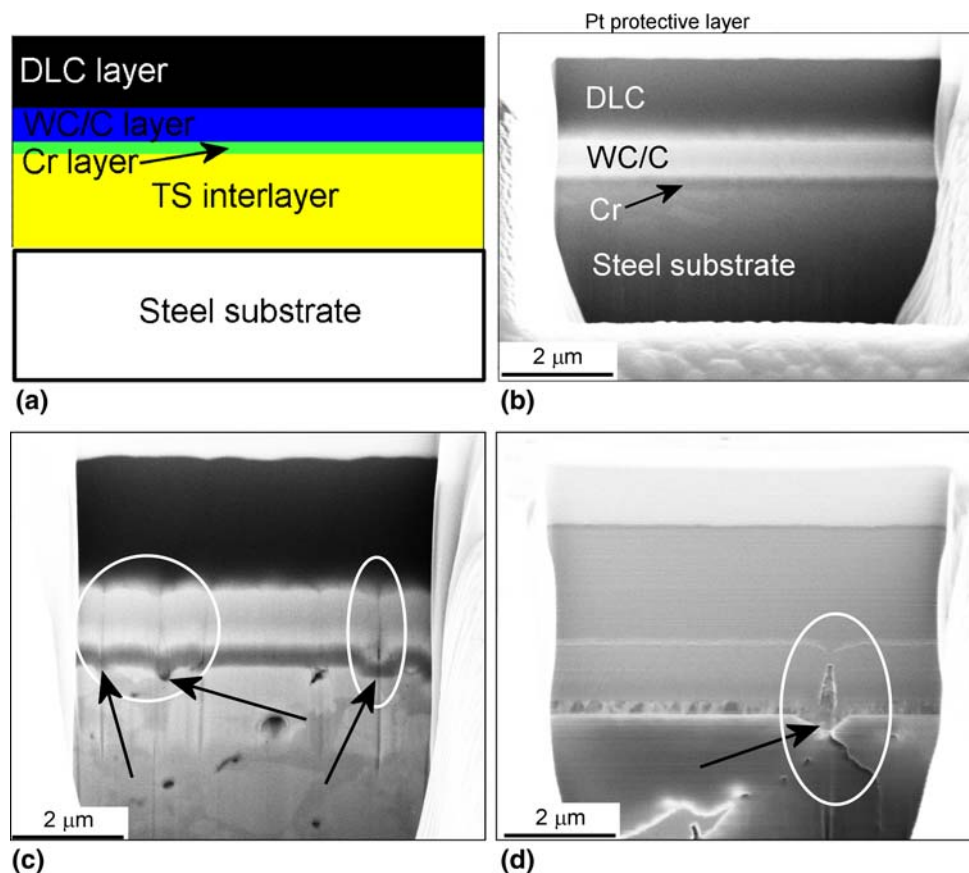


Fig. 1 (a) General layout of the multi-layer coating system comprising a thermally sprayed interlayer and a three-layer thin film. (b) SEM image (secondary electrons, e-beam acceleration voltage 5 kV, tilt angle 52°) of the FIB section of the thin film deposited on the bare C40 substrate. (c) SEM image (secondary electrons, e-beam acceleration voltage 5 kV, tilt angle 52°) of the FIB section of the thin film deposited on the HVOF-sprayed WC-17%Co interlayer. The circles indicate defects in the Cr and WC/C layers, due to the imperfections on the polished WC-Co surface pointed out by arrows. (d) FIB image (ion beam detector, ion beam current 5 pA, tilt angle 52°) of the FIB section of the thin film deposited on APS Al₂O₃-TiO₂. The circle indicates a defect in the Cr and WC/C layers, due to an imperfection on the polished interlayer surface pointed out by an arrow

(Conscan Profilometer, CSM Instruments), the wear rates of the pins were determined by measuring the diameter of the worn cap using an optical microscope, and the friction coefficient was monitored online during the test, using a load cell. The wear scars on the coated samples were also observed and sectioned using the SEM + FIB dual beam machine.

Anodic and cathodic electrochemical polarization tests were performed on polished uncoated C40, on polished thermally sprayed layers and on all DLC-based thin films. The tests were performed in contact with a 0.1 M HCl aqueous solution in equilibrium with the environment at room temperature, using a three-electrode cell (K0235 flat cell, Princeton Applied Research) where the sample is the working electrode, the counter electrode is a Pt grid and the reference electrode is an Ag/AgCl electrode. The sample is pressed against a Teflon gasket leaving a 1 cm² exposed surface. An Ametek VersaStat3 potentiostat-galvanostat (Princeton Applied Research, UK) was employed. The scanned potential range is -400 mV/+400 mV from rest potential, at a scan rate of 0.2 mV/s. The tests commenced after 30 min of free corrosion

Table 1 Chemical composition of the DLC top layer, as determined by XPS analysis

	C, at.%	O, at.%	% sp ³
DLC as-deposited	91	9	70 ± 4
DLC after the tribological test at 300 °C	86	14	60 ± 4

(to allow full wetting of the coating surface and open circuit potential stabilization). The corrosion current density I_{corr} (A/cm²) and corrosion potential E_{corr} (mV) were determined by Tafel analysis.

3. Results and Discussion

3.1 Microstructure, Chemical Composition, and Micromechanical Properties of the Thin Film

All of the DLC top layers have an identical chemical composition, listed in Table 1, irrespective of the nature of the underlying surface. No detectable impurities are

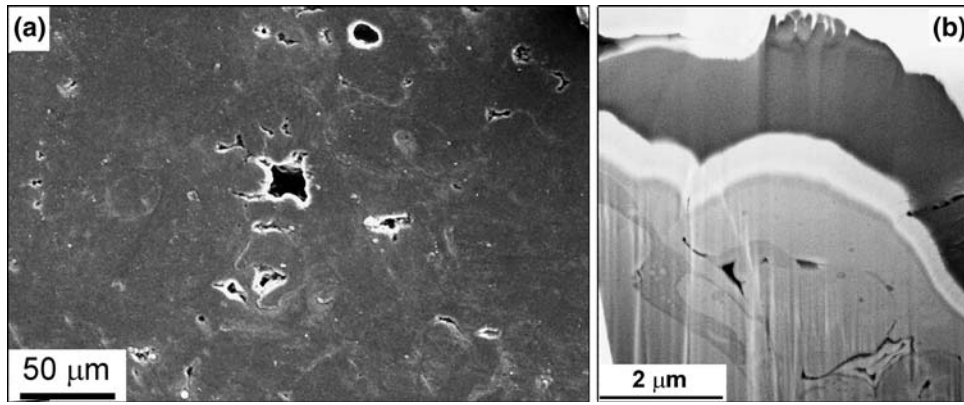


Fig. 2 SEM image (secondary electrons, e-beam acceleration voltage 15 kV, tilt angle 0°) of the top surface of the DLC-based thin film on the Ni-50%Cr interlayer (a) and SEM image (secondary electrons, e-beam acceleration voltage 5 kV, tilt angle 52°) of the FIB section of a small pore (b)

present, except for oxygen, which is probably due to surface contamination. The sp^3/sp^2 ratio is quite high (Ref 1).

Neither along the interface between the thin-film coatings and the polished thermally sprayed interlayers, nor along the thin film-C40 interface can large defects be noted (Fig. 1b-d). The three layers composing the films, namely DLC, WC/C, and Cr, are clearly recognizable in the FIB-produced cross sections and show sharp interfaces.

On the very smooth surface of the polished C40 steel, the multi-layer thin film can grow free of any apparent defect (Fig. 1b). By contrast, small imperfections exist on the polished surfaces of the thermally sprayed interlayers: for example, on the $Al_2O_3-TiO_2$ layer, imperfections are often due to brittle cracking during grinding and polishing (Fig. 1d, see arrow), whereas on the WC-Co one, imperfections arise because the abrasion rate of the soft Co matrix is larger than that of the hard carbide particles (Fig. 1c, see arrows). These small imperfections induce defects in the sputtered Cr and WC/C layers (Fig. 2c and d, see circles), but such defects do not extend to the DLC layer. The smooth DLC top layer can therefore preserve the very low roughness of the polished C40 and WC-Co surfaces (Table 2).

As the DLC films deposited on different surfaces have analogous chemical composition and sp^3/sp^2 ratio, their average nanohardness values are also very similar (Table 2), if the related standard deviation values are considered. As the indentation depth (200 nm) is less than 10% of the thickness of the DLC top layer, those values may be considered representative of its intrinsic hardness (Ref 25, 26). However, it may be noted that the hardness values of the films deposited on thermally sprayed interlayers exhibit a somewhat higher standard deviation. The homogeneity of the mechanical properties of the DLC layers might therefore have been influenced by the above-mentioned irregularities on the polished surfaces of the thermally sprayed interlayers, although the film's microstructure seemed not to be remarkably affected.

Table 2 Average roughness (R_a) and Berkovich nanohardness (H) of the DLC-based thin films deposited onto the various polished surfaces

	DLC on C40	DLC on WC-Co	DLC on $Al_2O_3-TiO_2$	DLC on NiCr
R_a , μm	0.0301	0.0401	0.183	0.157
H , GPa	19.1 ± 1.4	20.1 ± 3.3	20.0 ± 3.6	19.5 ± 2.7

The roughness of the polished APS surfaces is larger by one order of magnitude, as explained in Section 2.2; indeed, apart from the above-mentioned small imperfections, APS coatings also contain unavoidable porosity (Ref 27, 28), due to the intrinsic characteristics of the deposition technique (Ref 17). After surface polishing, open pores are therefore present on the surface of APS coatings: these open pores are much larger than the small polishing-induced imperfections shown in Fig. 1, so that the DLC film is clearly too thin to fill in and cover them completely (Fig. 2a), although it can be found inside some of them (Fig. 2b). Consequently, the thin film-coated APS layers retain their originally larger roughness (Table 2).

It should be remarked that, most probably, the standard deviation of the nanohardness values is not largely affected by the defectiveness of the thin films inside these large pores, as the indentations were performed on the smooth surface outside the pores.

3.2 Tribological Behavior

The evolution of the friction coefficient during the dry sliding ball-on-disk test performed at room temperature immediately indicates that the DLC-based thin film deposited on the $Al_2O_3-TiO_2$ interlayer is completely removed soon after the beginning of the wear test (Fig. 3a) and, accordingly, the final wear rate of both the coating and the counterpart is larger by several orders of magnitude than in all other cases (Fig. 3b). Brittle failure of the $Al_2O_3-TiO_2$ interlayer is clearly seen on the wear scar produced after a sliding distance of only 500 m

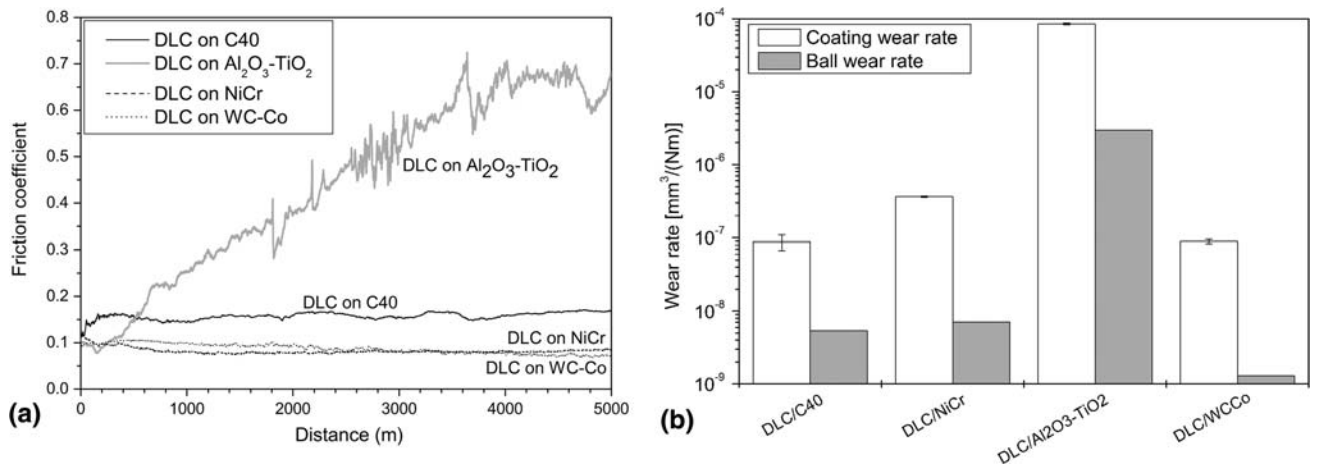


Fig. 3 Friction coefficient recorded during room temperature ball-on-disk tests (a) and wear rates of samples and counterparts (b)

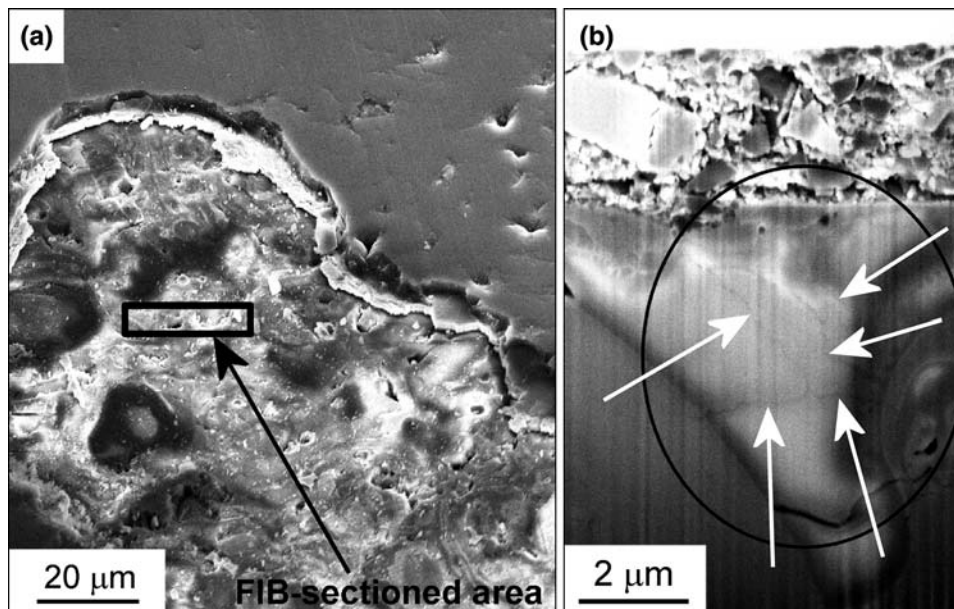


Fig. 4 Wear scar produced after 500 m sliding at room temperature on the DLC/Al₂O₃-TiO₂ system. (a) SEM image (secondary electrons, e-beam acceleration voltage 15 kV, tilt angle 52°) of the top surface, showing spallation due to brittle failure of the Al₂O₃-TiO₂ interlayer. The rectangle indicates the area subsequently subjected to FIB sectioning. (b) SEM image (secondary electrons, e-beam acceleration voltage 5 kV, tilt angle 52°) of the FIB section produced inside the spalled region. The circle and the arrows indicate the presence of a network of microcracks below the polished surface of the interlayer

(Fig. 4a); sectioning of that brittle failure area by the FIB technique reveals that, under a thin layer of wear debris, the Al₂O₃-TiO₂ ceramic is severely microcracked (Fig. 4b, see circle and arrows). This means that delamination is not caused by failure in the thin film or at the interface, but inside the ceramic layer itself. Such layer is indeed very brittle: its indentation fracture toughness is (1.66 ± 0.45) MPa·m^{1/2} (Ref 19), both because of its ceramic nature and because it contains numerous defects, as the large amount of open porosity produced after polishing clearly indicates. It is therefore unable to stand the current contact conditions, which are particularly severe: for instance,

application of the Hertz's theory indicates that the average contact pressure which would be produced on a bare steel surface under these conditions is about 1780 MPa.

Although the improper growth of the thin film inside the open pores of the polished Al₂O₃-TiO₂ would have been expected to result in local weakness of the film itself, the previous observations reveal that this is far surpassed by the brittleness of the interlayer, and by the stress concentration effects which those defects induce inside this interlayer.

Consistently, scratch test results (which had been discussed previously in Ref 15, as well) also suggest that the

brittleness of the interlayer plays a dominant role, while the effect of film imperfections inside the open pores is not particularly important. The tensile cracks occurring at the L_{C1} critical load (Fig. 5), indeed, do not exhibit major interactions with such open pores (Fig. 6b). Moreover, brittle failure of the interlayer occurs when the normal load becomes sufficiently large (see SEM micrograph in Fig. 6c: the EDX microanalysis in Fig. 6d confirms that the fracture occurred within the interlayer); indeed, an L_{C3} value could be detected (Fig. 5), although the scratch failure maps reported in the pertinent literature (Ref 29), which are based on the film/substrate hardness ratio

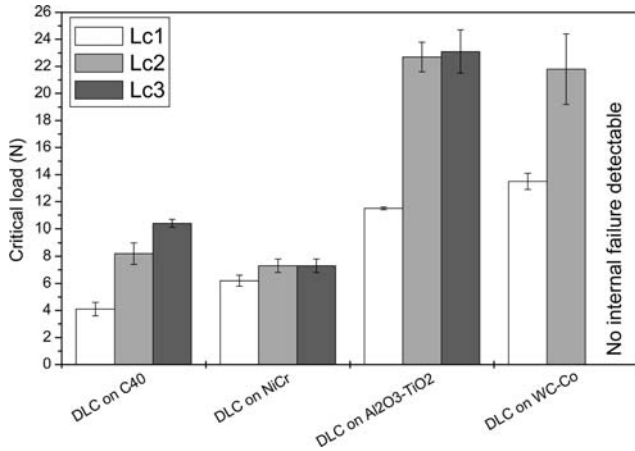


Fig. 5 Critical loads measured by scratch testing

(equal to 2.9 in the present configuration, with a substrate hardness of 6.9 GPa (Ref 15) and the film hardness in Table 2), would have predicted no complete coating breakthrough in the 0.1-30 N load range.

By contrast, the DLC-based film deposited onto the WC-Co interlayer has not undergone any cracking or spalling during the whole sliding test at room temperature (Fig. 7a). The WC-Co interlayer indeed possesses very high hardness (10.4 GPa (Ref 15)), capable of providing excellent support to the hard and brittle top layer, as shown by the scratch test results in Fig. 5. In this case, indeed, no L_{C3} critical load could be identified, consistently with the prediction from scratch maps (Ref 29). This interlayer is also substantially tougher than the APS oxide ceramic, so that no cracking or alterations can be highlighted by FIB sections (compare Fig. 7b to Fig. 1c). The DLC top layer has simply undergone mild polishing wear (Fig. 7a), which is typical of DLC films when their substrate does not yield (Ref 13, 30, 31). Under these conditions, DLC films can express their tribological qualities at their best; accordingly, both the coating and the counterbody exhibit the lowest wear rates (Fig. 3b), and the friction coefficient eventually attains the lowest value (Fig. 3a).

The DLC-based thin films on the NiCr interlayer and on the bare C40 substrate exhibit microcracking and localized spallation (Fig. 8a and b). Accordingly, in both cases, the critical loads found after scratch testing are substantially lower than those for the WC-Co/thin film system (Fig. 5). Microcracking and local spallation during wear testing are known to occur when the substrate yields

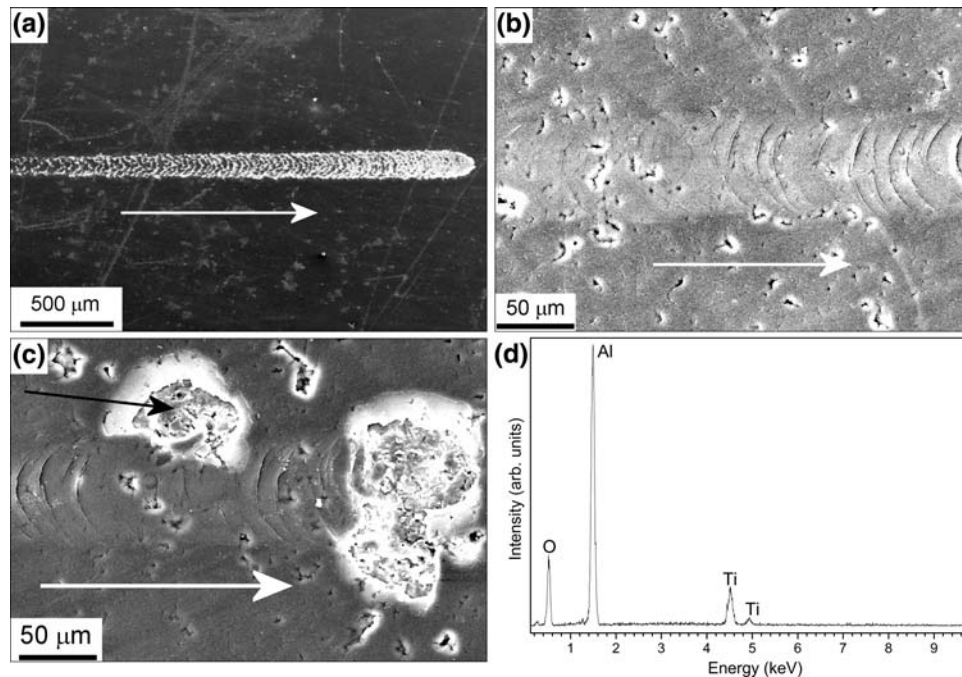


Fig. 6 SEM micrographs (secondary electrons) of the scratch grooves on (a) the DLC/C40 system (e-beam acceleration voltage 15 kV, tilt angle 0°) and (b, c) on the DLC/Al₂O₃-13%TiO₂ system (e-beam acceleration voltage 25 kV, tilt angle 0°); (d) EDX analysis of the spalled area which is indicated by the black arrow in (c). The white arrows indicate the scratch direction

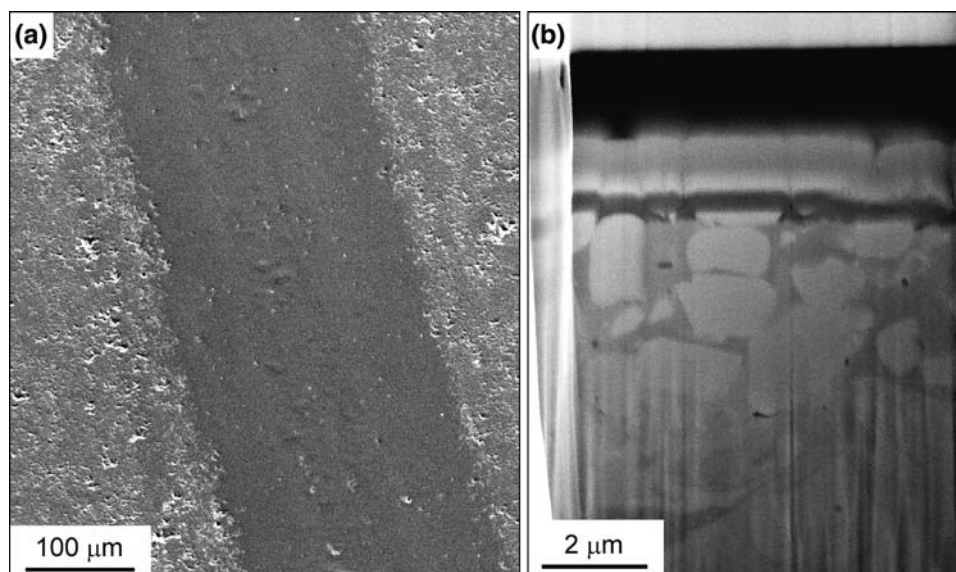


Fig. 7 Wear scar produced after 5000 m sliding at room temperature on the DLC/WC-Co system. (a) SEM image (secondary electrons, e-beam acceleration voltage 15 kV, tilt angle 52°) of the top surface showing mild abrasion of the DLC top layer. (b) SEM image (secondary electrons, e-beam acceleration voltage 5 kV, tilt angle 52°) of the FIB section produced inside the wear scar

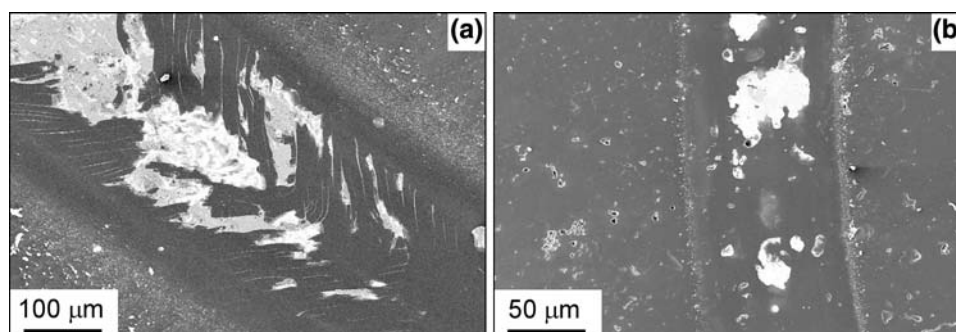


Fig. 8 SEM images (secondary electrons, e-beam acceleration voltage 5 kV, tilt angle 0°) of the wear scars produced after 5000 m sliding at room temperature on the DLC/C40 (a) and DLC/Ni-Cr (b) systems

under the applied contact pressure (Ref 7, 30). Extensive yielding of these soft substrates (the average hardness of NiCr and C40 is 3.3 and 3.1 GPa, respectively (Ref 15)) under contact conditions is also revealed by the remarkable buckling failure occurring during scratch testing (Fig. 6b).

It is interesting to note that the thin film/NiCr system has somewhat lower L_{C2} and L_{C3} values than the thin film/C40 system, in spite of the slightly lower hardness of the C40 substrate. This is probably a consequence of the presence of defects and pores on the polished surface of the NiCr layer, which slightly anticipate the onset of cracking.

Previous literature indicates that the above-described wear mechanism, based on localized spallation, is characteristic of a “borderline” situation: if contact conditions become only slightly more severe, complete delamination of the DLC-based film occurs (Ref 7, 30). Due to this local spallation, the wear rates of the coated sample and of the

ball are larger than in the case of the WC-Co interlayer (Fig. 3b). Moreover, the friction coefficient produced by the DLC-based film deposited on the bare C40 surface is somewhat higher (about 0.15) than the one produced by the film on WC-Co (Fig. 3a).

Increasing the temperature to 300 °C reduces the hardness and the load carrying capacity of the C40 steel substrate and of the NiCr interlayer; consequently, contact conditions become more severe and, as anticipated earlier, complete delamination of the DLC-based thin film occurs well before the end of the 5000-m-long tribological test (Fig. 9). Whereas this result was expected and easily explainable, interpretation of the behavior of the films deposited on the WC-Co and on the Al_2O_3 - TiO_2 interlayers is less straightforward (Fig. 9). The performance of these two layers is indeed reversed: the film on the Al_2O_3 - TiO_2 substrate never delaminates completely and retains a quite stable friction coefficient, whereas the film on the WC-Co interlayer comes to a complete delamination,

even though after a much longer sliding distance than the films on C40 and on NiCr.

FIB sections suggest that the behavior of the two thermally sprayed interlayers is deeply modified. By sectioning the wear scar of the film on the $\text{Al}_2\text{O}_3\text{-TiO}_2$ interlayer at the end of the 5000-m-long sliding test, it is noted that cracking of the interlayer is significantly reduced (compare Fig. 10a to Fig. 4b), so that spallation due to failure of the ceramic interlayer is largely prevented. It would therefore seem that the toughness of the ceramic interlayer is increased at 300 °C, whereas its hardness is not remarkably impaired. Literature data concerning the high-temperature toughness of alumina

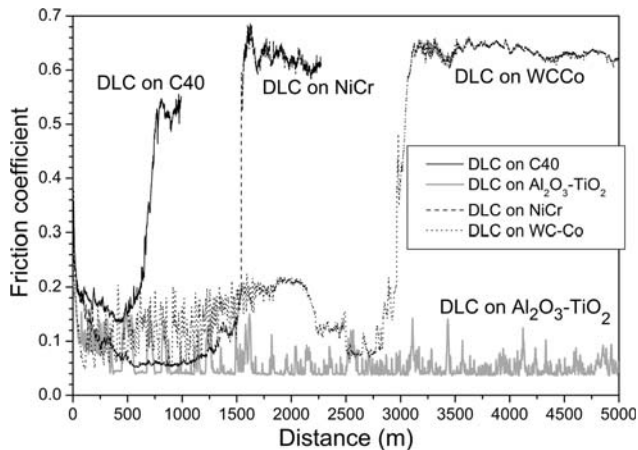


Fig. 9 Friction coefficient recorded during ball-on-disk tests at 300 °C

ceramics, especially thermally sprayed ones, are scarce; however, some papers suggest that their toughness could actually increase with increasing temperature (Ref 32).

In contrast, by sectioning the wear groove of the film on the WC-Co interlayer after a sliding distance of 2000 m (i.e. slightly before the delamination of the DLC film, Fig. 10b), a remarkable alteration in the WC-Co layer's microstructure is apparent (compare Fig. 10b to Fig. 1c and 7b). Specifically, it seems that the carbide grains have been fractured and comminuted (Fig. 10b, circle). It might be speculated that, at 300 °C, the hardness of the Co matrix definitely decreases; therefore, the metal matrix yields and most of the contact stresses are distributed on the WC particles, which become overloaded and undergo brittle fracture. The plastic flow of the metal matrix subsequently embeds the comminuted carbide fragments and gives rise to the morphology seen in Fig. 10(b).

It can also be noted that the friction coefficient exhibited by the DLC-based thin film on the $\text{Al}_2\text{O}_3\text{-TiO}_2$ interlayer at 300 °C (Fig. 9), even though quite stable, is not as stable as the friction coefficient trends recorded at room temperature (Fig. 3a). First, some very limited spallation phenomena still occur (Fig. 11, circle). Secondly, at the end of the 5000-m-long test, the DLC top layer is slightly grooved (Fig. 11) and considerably thinned. The decrease in the top layer's thickness can be noted both by the FIB section (Fig. 10a) and by SEM micrographs of the top surface (Fig. 11): indeed, lighter color is seen in the middle of the wear track, meaning that the DLC top layer has become so thin that the emitted secondary electrons come also from the underlying WC/C layer, which has a significantly larger average atomic weight and consequently produces a brighter contrast.

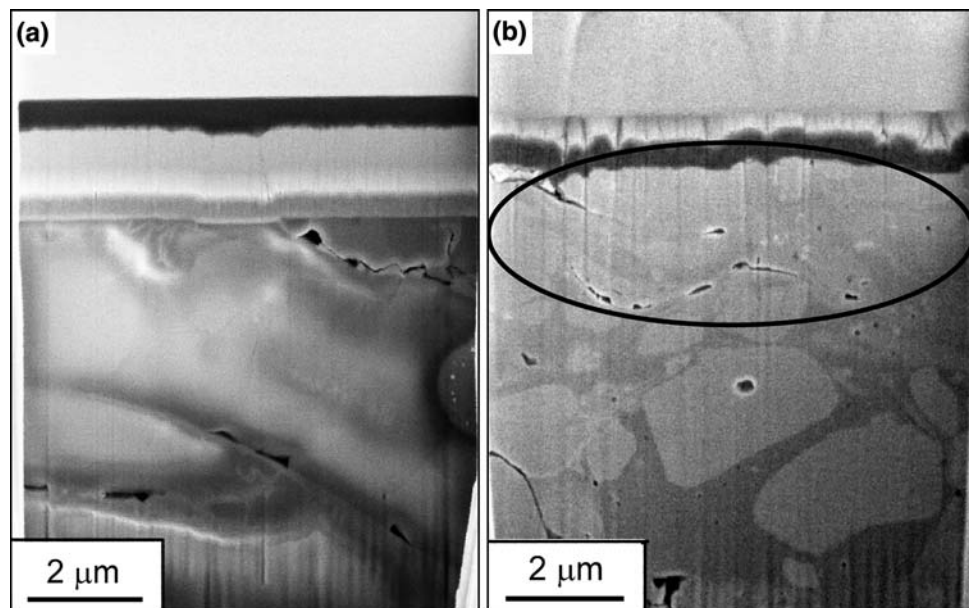


Fig. 10 SEM images (secondary electrons, e-beam acceleration voltage 5 kV, tilt angle 52°) of the FIB sections of the wear scars produced at 300 °C on the DLC/ $\text{Al}_2\text{O}_3\text{-TiO}_2$ system after 5000 m sliding distance (a) and on the DLC/WC-Co system after 2000 m sliding distance (b). The circle indicates microstructural alterations in the WC-Co layer

The grooving and the significant reduction in thickness suggest that the wear resistance of the DLC top layer is somewhat impaired at 300 °C. Accordingly, XPS chemical

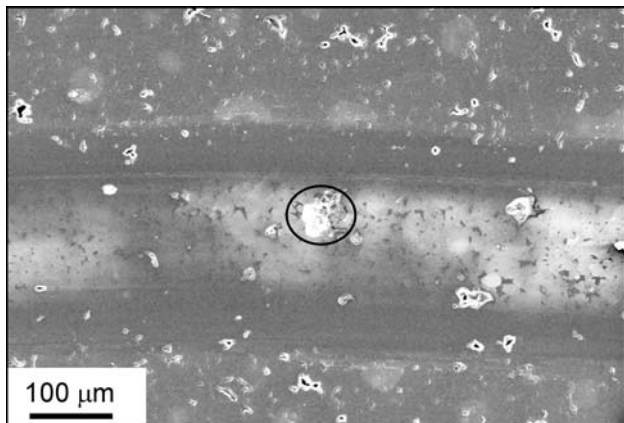


Fig. 11 SEM image (secondary electrons, e-beam acceleration voltage 15 kV, tilt angle 0°) of the wear scar produced after 5000 m sliding at 300 °C on the DLC/Al₂O₃-TiO₂ system. The circle indicates a small spalled area

analyses performed on the coated samples after the 300 °C tribological test indicate a decrease in the sp³/sp² ratio (Table 1). This change, which is likely a consequence of temperature-induced transformations, probably reduces the hardness of the DLC top layer. The increased rate of material removal from the DLC film and its altered chemical composition can explain the less stable friction coefficient trend.

3.3 Electrochemical Polarization Testing

The electrochemical polarization curves and the results of Tafel's analysis indicate that the two APS-deposited interlayers (both the NiCr one and the Al₂O₃-TiO₂ one), by themselves, do not enhance the corrosion resistance of the C40 substrate remarkably (Fig. 12a, c, and d; Table 3). The limited protectiveness of APS coatings against aqueous corrosion is a well-known issue, largely documented by several previous studies (Ref 33-35). These coatings, indeed, contain a certain amount of open and interconnected pores, allowing the diffusion of the electrolyte down to the steel substrate. Moreover, in the NiCr coating, the oxidation of the metallic lamellae (as shown

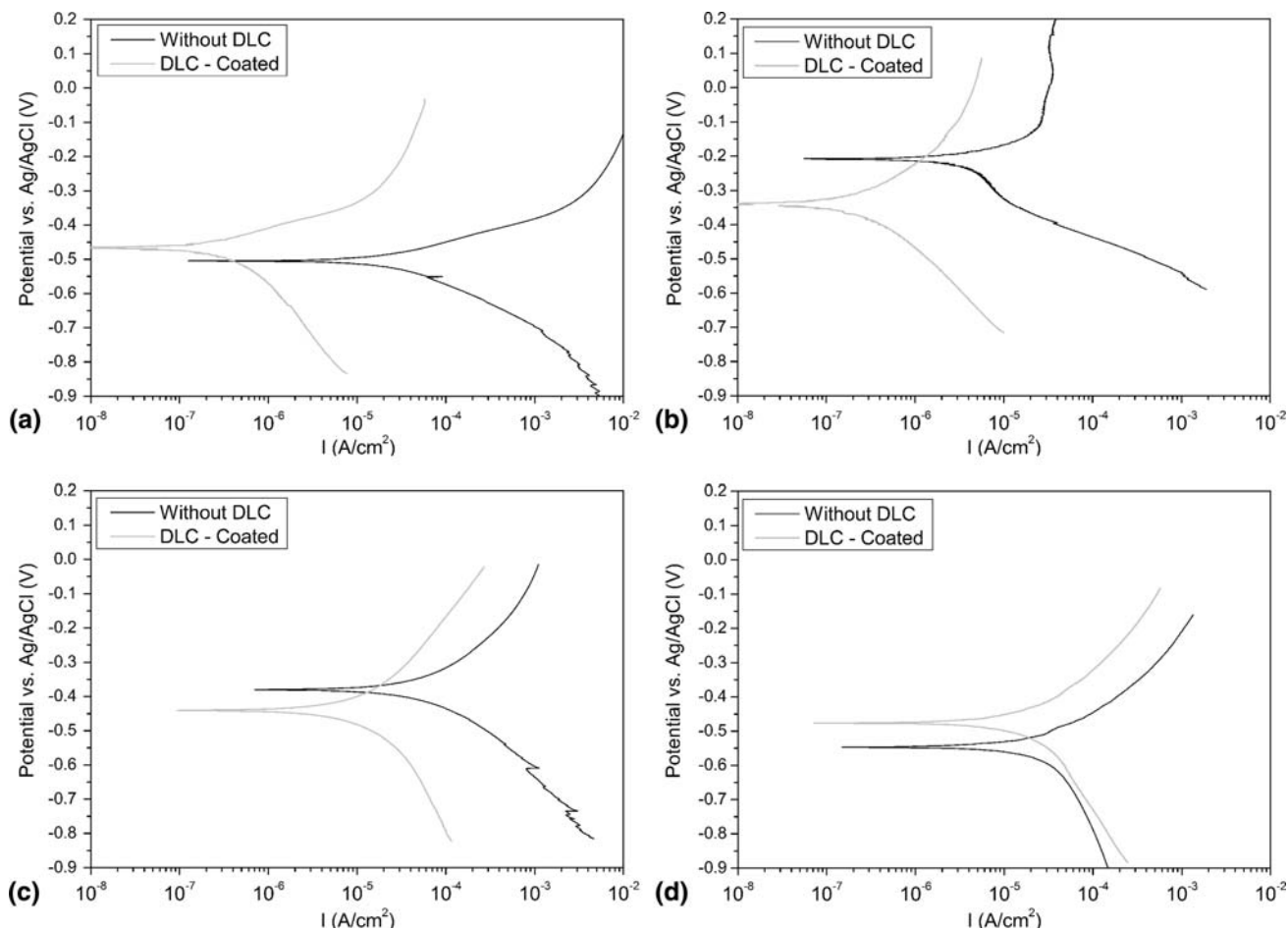


Fig. 12 Electrochemical polarization curves of uncoated and thin film-coated C40 (a), WC-Co (b), NiCr (c), and Al₂O₃-TiO₂ (d) samples

in Fig. 13) impairs the material's intrinsic corrosion resistance: as thoroughly described in previous papers (Ref 36, 37), this oxidation phenomenon deprives the alloy of Cr, the element conferring passivation capabilities. The dense HVOF-deposited WC-Co coating, by contrast, protects the steel substrate from corrosion quite effectively (Fig. 12b and Table 3), as highlighted by many previous papers (Ref 35, 38-40).

The deposition of the DLC-based thin films produces distinct effects on different samples: when deposited onto the C40 and WC-Co surfaces, it shifts the polarization curves toward significantly lower current density values (Fig. 12a and b) and it accordingly reduces the corrosion current density by one or two orders of magnitude (Table 3). It has indeed previously been shown that the DLC top layer produced onto the C40 and WC-Co surfaces possesses a very low defectiveness (Section 3.1, Fig. 1); therefore, it provides an excellent physical barrier against the penetration of external corrosive agents, thanks to its intrinsic chemical inertness. The thin film/WC-Co system consequently exhibits the lowest corrosion current density: indeed, the dense cermet layer protects the steel substrate from the small amount of electrolyte which can pass through the few defects in the thin film.

By contrast, the thin film produces little beneficial effects when deposited onto the APS interlayers (Fig. 12c and d and Table 3). These layers were indeed shown to possess many open pores, which the thin film could not fill completely, although it could partly enter some of them (Section 3.1, Fig. 2): the electrolyte can still penetrate

through these pores, a large part of which remain open, and reach the steel substrate.

4. Conclusions

“Duplex” systems consisting of a three-layer DLC-based thin film deposited onto different thermally sprayed interlayers (namely Ni-50%Cr, Al_2O_3 -13% TiO_2 , and WC-17%Co) were subjected to ball-on-disk tests, both at room temperature and at 300 °C, and were analyzed by the FIB technique, both in the as-deposited condition and after tribological testing.

The results indicate that the hardness of the interlayer is of primary importance: a relatively soft interlayer, like the Ni-50%Cr one, does not improve the sliding wear behavior of the DLC-based film. However, the toughness of the interlayer is also very important: at room temperature, the hard but very brittle Al_2O_3 -13% TiO_2 interlayer fails under severe contact conditions, thus leading to complete removal of the film. Consequently, at room temperature, the hard and tough WC-17%Co cermet interlayer offers the best performance; indeed, it can bear the contact stress distribution with no perceivable microstructural alteration and, consequently, it succeeds in preventing any cracking and spallation phenomena of the thin film.

At 300 °C, the presence of a hard interlayer is even more important, because the load-carrying capability of the steel substrate is further impaired, so that full delamination of the coating soon occurs. Contrarily to the room temperature conditions, the best performing interlayer at 300 °C is the Al_2O_3 -13% TiO_2 one; indeed, brittle fracture of the interlayer seems largely reduced. By contrast, the WC-17%Co interlayer suffers a microstructural alteration, because of the combined effect of the severe contact stress and of the high temperature. Therefore, it partly loses its load-carrying ability and it cannot prevent the delamination of the film, although delamination occurs later than on the bare steel substrate.

It is also noted that, at 300 °C, the sp^3/sp^2 ratio of the DLC top layer decreases and its intrinsic tribological properties are slightly degraded.

The corrosion behavior of the duplex systems was also investigated: as the polished APS interlayers show a significant amount of open, interconnected pores, the thin film is unable to fill and close them completely (although it can enter part of them), so that it cannot act as a physical barrier against the penetration of external corrosive agents. By contrast, the DLC top layer is almost free of any large defect when deposited onto smooth surfaces, as

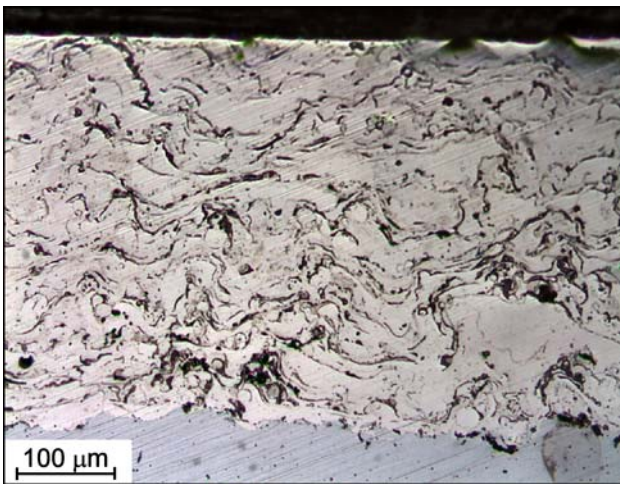
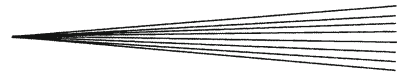


Fig. 13 Optical micrograph of the polished cross section of the Ni-50%Cr layer

Table 3 Corrosion current density (I_{corr} , $\mu\text{A}/\text{cm}^2$) and corrosion potential (E_{corr} , mV) of thin film-coated and uncoated samples

	C40	DLC on C40	NiCr	DLC on NiCr	Al_2O_3 - TiO_2	DLC on Al_2O_3 - TiO_2	WC-Co	DLC on WC-Co
I_{corr}	87.5	0.982	66.4	17.6	37.5	23.9	3.82	0.274
E_{corr}	-564	-547	-374	-410	-531	-483	-215	-314



the polished C40 and WC-Co ones. In this case, the film offers an excellent barrier against the outer environment and enhances the corrosion resistance of the system significantly. Therefore, the thin film/WC-Co system displays the lowest corrosion current density, thanks to the combined action of the defect-free film and of the corrosion-resistant interlayer.

Acknowledgments

The authors acknowledge the deposition of thermally sprayed coatings by Dr. Fabrizio Casadei, Mr. Edoardo Severini, Mr. Francesco Barulli, Mr. Valerio Ferretti (Centro Sviluppo Materiali S.p.A., Roma, Italy). Many thanks to Ing. Andrea Bassani and Mr. Binit Kumar for their assistance with the characterization tests and to Dr. Monica Montecchi and Dr. Luca Pasquali for the XPS analyses. Thanks to Dr. Gian Carlo Gazzadi for the assistance during FIB sessions. This work was partly supported by PRRIITT (Regione Emilia-Romagna), Net-Lab SUP&RMAN (Surfaces & Coatings for Advanced Mechanics and Nanomechanics).

References

1. D.W. Wheeler, Chemical Vapour Deposition Methods for Protection Against Wear. *Surface Coatings for Protection Against Wear*, B.G. Mellor, Ed., Abington Hall, Cambridge, UK: Woodhead Publishing Limited, 2006, p 129
2. F.E. Kennedy, D. Lidhagen, A. Erdemir, J.B. Woodford, and T. Kato, Tribological Behaviour of Hard Carbon Coatings on Steel Substrates, *Wear*, 2003, **255**, p 854-858
3. G.A. Jones, On the Tribological Behaviour of Mechanical Seal Face Materials in Dry Line Contact: Part II. Bulk Ceramics, Diamond and Diamond-Like Carbon Films, *Wear*, 2004, **256**, p 433-455
4. A. Leyland and A. Matthews, On the Significance of the H/E Ratio in Wear Control: A Nanocomposite Coating Approach to Optimised Tribological Behaviour, *Wear*, 2000, **246**, p 1-11
5. K. Holmberg, A. Laukkanen, H. Ronkainen, K. Wallin, S. Varjus, and J. Koskinen, Tribological Contact Analysis of a Rigid Ball Sliding on a Hard Coated Surface: Part II: Material Deformations, Influence of Coating Thickness and Young's Modulus, *Surf. Coat. Technol.*, 2006, **200**, p 3810-3823
6. S.A.G. Oliveira and A.F. Bower, An Analysis of Fracture and Delamination in Thin Coatings Subjected to Contact Loading, *Wear*, 1996, **198**, p 15-32
7. J. Jiang, R.D. Arnell, and J. Tong, Some Special Tribological Features of DLC Coatings Deposited on Soft Substrates, *Wear*, 1997, **211**, p 254-264
8. B. Podgornik and J. Vižintin, Influence of Substrate Treatment on the Tribological Properties of DLC Coatings, *Diamond Relat. Mater.*, 2001, **10**, p 2232-2237
9. Y. Liu and E.I. Meletis, Tribological Behavior of DLC Coatings with Functionally Gradient Interfaces, *Surf. Coat. Technol.*, 2002, **153**, p 178-183
10. R. Gadow and D. Scherer, Composite Coatings with Dry Lubrication Ability on Light Metal Substrates, *Surf. Coat. Technol.*, 2000, **151-152**, p 471-477
11. F. Casadei, R. Pileggi, R. Valle, and A. Matthews, Studies on a Combined Reactive Plasma Sprayed/Arc Deposited Duplex Coating for Titanium Alloys, *Surf. Coat. Technol.*, 2006, **201**, p 1200-1206
12. E. Bemporad, M. Sebastiani, F. Casadei, and F. Carassiti, Modelling, Production and Characterisation of Duplex Coatings (HVOF and PVD) on Ti-6Al-4 V Substrate for Specific Mechanical Applications, *Surf. Coat. Technol.*, 2007, **201**, p 7652-7662
13. X. Nie, A. Wilson, A. Leyland, and A. Matthews, Deposition of Duplex Al_2O_3 /DLC Coatings on Al Alloys for Tribological Applications Using a Combined Micro-Arc Oxidation and Plasma-Immersion Ion Implantation Technique, *Surf. Coat. Technol.*, 2000, **131**, p 506-513
14. S.H. Awad and H.C. Qian, Deposition of Duplex Al_2O_3 /TiN Coatings on Aluminum Alloys for Tribological Applications Using a Combined Microplasma Oxidation (MPO) and Arc Ion Plating (AIP), *Wear*, 2006, **260**, p 215-222
15. G. Bolelli, L. Lusvarghi, F. Pighetti Mantini, F. Pitacco, and H. Volz, Enhanced Tribological Properties of PECVD DLC Coated Thermally Sprayed Coatings, *Surf. Coat. Technol.*, 2008, **202**, p 4382-4386
16. J.M. Guilemany and J. Nin, Thermal Spraying Methods for Protection Against Wear. *Surface Coatings for Protection Against Wear*, B.G. Mellor, Ed., Abington Hall, Cambridge, UK: Woodhead Publishing Limited, 2006, p 249
17. H. Herman, S. Sampath, and R. McCune, Thermal Spray: Current Status and Future Trends, *MRS Bull.*, 2000, **25(7)**, p 17-25
18. J.R. Davis, *Handbook of Thermal Spray Technology*, ASM International, Materials Park, OH, USA, 2004, p 169
19. G. Bolelli, V. Cannillo, L. Lusvarghi, and T. Manfredini, Wear Behaviour of Thermally Sprayed Ceramic Oxide Coatings, *Wear*, 2006, **261**, p 1298-1315
20. G. Bolelli, V. Cannillo, L. Lusvarghi, and S. Riccò, Mechanical and Tribological Properties of Electrolytic Hard Chrome and HVOF-Sprayed Coatings, *Surf. Coat. Technol.*, 2006, **200**, p 2995-3009
21. J. Jiang and R.D. Arnell, The Effect of Substrate Surface Roughness on the Wear of DLC Coatings, *Wear*, 2000, **239**, p 1-9
22. J.C. Lascovich, R. Giorgi, and S. Scaglione, Evaluation of the sp^2/sp^3 Ratio in Amorphous Carbon Structure by XPS and XAES, *Appl. Surf. Sci.*, 1991, **47**, p 17-21
23. W.C. Oliver and G.M. Pharr, An Improved Technique for Determining Hardness and Elastic Modulus Using Load and Displacement Sensing Indentation Experiments, *J. Mater. Res.*, 1992, **7**, p 1564-1583
24. S.J. Bull, Failure Modes in Scratch Adhesion Testing, *Surf. Coat. Technol.*, 1991, **50**, p 25-32
25. P.J. Burnett and D.S. Rickerby, The Mechanical Properties of Wear-Resistant Coatings: I: Modelling of Hardness Behaviour, *Thin Solid Films*, 1987, **148**, p 41-50
26. J. Lesage, A. Pertuz, E.S. Puchi-Cabrera, and D. Chicot, A Model to Determine the Surface Hardness of Thin Films from Standard Micro-Indentation Tests, *Thin Solid Films*, 2006, **497**, p 232-238
27. G. Antou, G. Montavon, F. Hlawka, A. Cornet, and C. Coddet, Exploring Thermal Spray Gray Alumina Coating Pore Network Architecture by Combining Stereological Protocols and Impedance Electrochemical Spectroscopy, *J. Therm. Spray Technol.*, 2006, **15**, p 765-772
28. G. Antou, G. Montavon, F. Hlawka, A. Cornet, and C. Coddet, Characterizations of the Pore-Crack Network Architecture of Thermal-Sprayed Coatings, *Mater. Charact.*, 2004, **53**, p 361-372
29. K.H. Lau, K.Y. Li, and Y.-W. Mai, Influence of Hardness Ratio on Scratch Failure of Coatings, *Int. J. Surf. Sci. Eng.*, 2007, **1**, p 3-21
30. J. Jiang, R.D. Arnell, and J. Tong, The Effect of Substrate Properties on Tribological Behaviour of Composite DLC Coatings, *Tribol. Int.*, 1997, **30**, p 613-625
31. D.-H. Kim, H.-E. Kim, K.-R. Lee, C.-N. Whang, and I.-S. Lee, Characterization of Diamond-Like Carbon Films Deposited on Commercially Pure Ti and Ti-6Al-4 V, *Mater. Sci. Eng. C*, 2002, **22**, p 9-14
32. E. Sánchez-González, P. Miranda, J.J. Meléndez-Martínez, F. Guiberteau, and A. Pajares, Temperature Dependence of Mechanical Properties of Alumina up to the Onset of Creep, *J. Eur. Ceram. Soc.*, 2007, **27**, p 3345-3349
33. A.A. Ashary and R.C. Tucker, Electrochemical Corrosion Studies of Alloys Plasma Sprayed with Cr_2O_3 , *Surf. Coat. Technol.*, 1989, **39-40**, p 701-709

34. M. Fukumoto, Y. Wada, M. Umemoto, and I. Okane, Effect of Connected Pores on the Corrosion Behavior of Plasma Sprayed Alumina Coatings, *Surf. Coat. Technol.*, 1989, **39-40**, p 711-720
35. G. Bolelli, V. Cannillo, R. Giovanardi, and L. Lusvarghi, Electrochemical Comparison Between Corrosion Resistance of Some Thermally Sprayed Coatings, *Int. J. Surf. Sci. Eng.*, 2008, **2(3-4)**, p 222-239
36. T.E. Lister, R.N. Wright, P.J. Pinhero, and W.D. Swank, Corrosion of Thermal Spray Hastelloy C-22 Coatings in Dilute HCl, *J. Therm. Spray Technol.*, 2002, **11**, p 530-535
37. D. Zhang, S.J. Harris, and D.G. McCartney, Microstructure Formation and Corrosion Behaviour in HVOF-Sprayed Inconel 625 Coatings, *Mater. Sci. Eng. A*, 2003, **344**, p 45-56
38. G. Bolelli, R. Giovanardi, L. Lusvarghi, and T. Manfredini, Corrosion Resistance of HVOF-Sprayed Coatings for Hard Chrome Replacement, *Corros. Sci.*, 2006, **48**, p 3375-3397
39. C. Monticelli, A. Frignani, and F. Zucchi, Investigation on the Corrosion Process of Carbon Steel Coated by HVOF WC/Co Cermets in Neutral Solution, *Corros. Sci.*, 2004, **46**, p 1225-1237
40. A. Neville and T. Hodgkiess, Corrosion Behaviour and Microstructure of Two Thermal Spray Coatings, *Surf. Eng.*, 1996, **12**, p 303-312